J. Fluid Mech. (2009), *vol.* 626, *pp.* 395–414.
doi:10.1017/S0022112009005990 Printed in the United Kingdom

Wave power extraction from an oscillating water column at the tip of a breakwater

HERVÉ MARTINS-RIVAS[1] AND CHIANG C. MEI[2]†

[1]Department of Aeronautics and Astronautics, Massachusetts Institute of Technology, Cambridge, MA 02139, USA

[2]Department of Civil and Environmental Engineering, Massachusetts Institute of Technology, Cambridge, MA 02139, USA

(Received 10 July 2008 and in revised form 29 December 2008)

To reduce the costs of construction, operation, maintenance, energy storage and grid connection, some devices for extracting energy from sea waves are likely to be installed on the coast. We study theoretically a single oscillating water column (OWC) installed at the tip of a long and thin breakwater. The linearized problems of radiation and scattering for a hollow cylinder with an open bottom are then solved by the usual method of eigenfunction expansions and integral equations. Since a thin breakwater is the limit of a wedge, an exact solution for the diffraction by a solid cylinder at the tip of a wedge is derived to facilitate the analysis. Following Sarmento & Falcão (*J. Fluid Mech.*, vol. 150, 1985, pp. 467–485), power takeoff by Wells turbines is modelled by including air compressibility in the chamber above the water surface. The effects of air compressibility on the extraction efficiency is studied. It is shown that for this simple geometry the angle of incidence affects the waves outside the structure but not the extracted power.

1. Introduction

The science and technology of power extraction from sea waves have been steadily advancing since the 1970s. Extensive reviews of existing devices can be found in Evans (1981), McCormick (1981), Mei (1983), Falcão (2002) and Falnes (2002). While many designs have been proposed, the most widely studied fall in two major types. In one, energy is collected from the oscillations of floating bodies such as buoys, cams and floats – see e.g. Salter (1974), Evans (1976), Mei (1976), Budal & Falnes (1977) and Newman (1979). The second type, called oscillating water column (OWC), consists of a stationary chamber open at the bottom that allows the water surface inside to push the dry air above through one or more Wells turbines which rotate in one direction only. For both types, optimum power absorption can in principle be achieved by impedance matching; i.e. the system must resonate at the design frequency, and the energy absorption rate must match the rate of radiation damping. In practice both the resonance frequency and the radiation damping rate are fixed once the device geometry is chosen. Because sea waves are random and broadband, a design challenge is to strive for high efficiency over a broad range of frequencies around the spectral peak of the incident sea. One way to achieve this is to manipulate the absorber by

† Email address for correspondence: ccmei@mit.edu

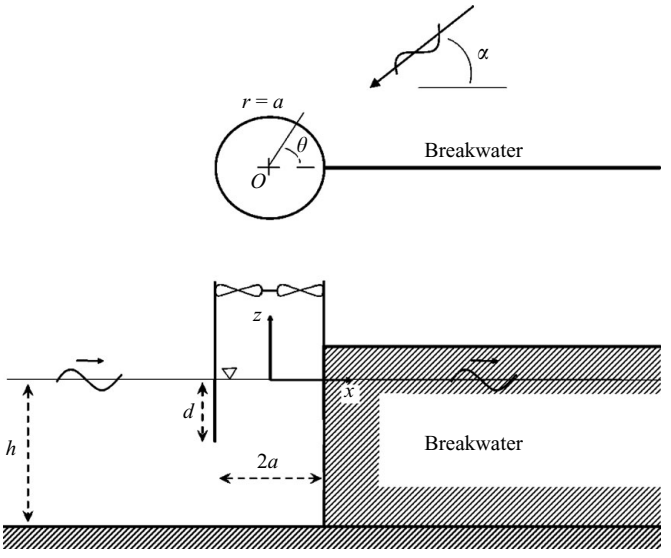

FIGURE 1. OWC at the head of a breakwater.

phase control (Budal & Falnes 1977). The other is to couple two or more mechanisms in one system so that multiple resonant peaks can be attained.

Theories for simple two-dimensional OWCs have been derived by Evans (1978, 1982), Smith (1983), Sarmento & Falcão (1985) and Evans & Porter (1995) who were the first to consider the compressibility of air inside the chamber. An isolated axisymmetric OWC in the open sea has been considered by Evans & Porter (1997) who modelled the system by a thin-walled circular cylinder with its open bottom elevated above the seabed, thus allowing waves to enter the column. The same boundary-value problem was studied earlier by Garrett (1970) for the diffraction by a bottomless harbour. In this case, the water surface inside the column is subjected only to the atmospheric pressure.

In general, siting of wave-energy absorbers depends not only on wave climate but also on different costs such as those of construction, operation, maintenance, storage and grid connection. For some projects it may be preferable to install the entire system on the coast rather than offshore. Since 1990 an experimental OWC pilot plant has been in operation on the coast of Pico Island of Azores, Portugal (Falcão 2000). New plans have been reported for another full-size OWC station at the head of a breakwater at the mouth of Foz do Douro River, Portugal (Martins *et al.* 2005). An OWC system of 300 MW capacity is being constructed at Mutrika city in the Basque country of northern Spain (Heath 2007). Effects of other types of coasts have been studied by McIver & Evans (1988) for a system of two-dimensional pistons oscillating at the end of identical harbours along a reflecting coast. Evans (1988) has derived formulas for the maximum power efficiency of devices near a straight coast line. So far no theory is known for an OWC on a breakwater.

In this paper we consider an idealized model of an OWC at the tip of a thin breakwater as sketched in figure 1. In order to examine the essential physics without massive numerical work, the sea depth is assumed to be constant everywhere. The more practical case of complex geometry and bathymetry can be dealt with by existing numerical means, as in Martins-Rivas & Mei (2007). Wells turbines are assumed to be installed on top of the cylindrical column. Special emphasis is on the effect of

air compressibility on the bandwidth of power-capture length. As is standard in the linearized theory, the hydrodynamic problem can be decomposed as the sum of radiation and diffraction problems. An exact solution for the diffraction by a solid cylinder at the tip of a wedge is described. It facilitates the analysis of the limiting case of a thin breakwater. A rather surprising result is that for this idealized geometry, the rate of energy extraction, which depends on the area average of the water surface displacement inside the column, is unaffected by the presence of the breakwater and hence is the same as for an OWC in the open sea. By virtue of an identity relating the diffraction and radiation problems, the extraction rate can be predicted by just solving the radiation problem alone.

2. Model of power takeoff

For the sake of convenience we first summarize the known relations between power takeoff and the hydrodynamic parameters needed. Let one or more Wells turbines be installed at the top of the cylinder. Due to the high sound speed in air and the low frequency of sea waves, the air pressure p_a is approximately uniform throughout the chamber. As in Evans (1982) we let the mass flux through the Wells turbines be proportional to the chamber air pressure. Following Sarmento & Falcão (1985), we further account for air compressibility and relate the mass flux of air to the turbine characteristics by

$$\frac{\mathrm{d}(\rho_a V)}{\mathrm{d}t} = \rho_a \frac{\mathrm{d}V}{\mathrm{d}t} + V\frac{\mathrm{d}\rho_a}{\mathrm{d}t} = \frac{KD}{N}\, p_a, \tag{2.1}$$

where N is the rotational speed of turbine blades, D the outer diameter of turbine rotor, ρ_a the air density and V the air chamber volume. The empirical coefficient K depends on the design, the number and set-up of turbines; $\mathrm{d}V/\mathrm{d}t$ is the linearized rate of total upward displacement of the water surface inside the column,

$$\frac{\mathrm{d}V}{\mathrm{d}t} = Q \equiv \iint_{S_c} w\ \mathrm{d}S = \int_0^a \int_0^{2\pi} w(r, \theta, z = 0, t)\ r\mathrm{d}r\ \mathrm{d}\theta, \tag{2.2}$$

where w denotes the vertical velocity of the water surface S_c in the chamber. Assuming isentropy so that $c_a^2(\mathrm{d}\rho_a/\mathrm{d}t) = \mathrm{d}p_a/\mathrm{d}t$, where c_a is the sound velocity in air, we have

$$\frac{\mathrm{d}(\rho_a V)}{\mathrm{d}t} = \rho_a^0 Q - \frac{V_o}{c_a^2}\frac{\mathrm{d}p_a}{\mathrm{d}t} \tag{2.3}$$

with ρ^0 being the air density. Then, for simple harmonic motion with $Q = \mathrm{Re}(\widehat{Q}\mathrm{e}^{-\mathrm{i}\omega t})$, $p_a = \mathrm{Re}(\widehat{p}_a \mathrm{e}^{-\mathrm{i}\omega t})$,

$$\widehat{Q} = \left(\frac{KD}{N\rho_a^0} - \frac{\mathrm{i}\omega V_o}{c_a^2 \rho_a^0}\right)\widehat{p}_a \tag{2.4}$$

as in Sarmento & Falcão (1985).

For small-amplitude waves the linearized velocity potential $\Phi \mathrm{e}^{-\mathrm{i}\omega t}$ in water can be treated as the sum of radiation and diffraction potentials, i.e.

$$\Phi(x, y, z) = \phi(x, y, z) + \varphi(x, y, z). \tag{2.5}$$

The radiation potential (ϕ) describes the water response to the oscillating air pressure inside the column. The diffraction potential (φ) is the response to a train of plane incident waves in the presence of the OWC/coast system. Accordingly, the upward flux at the water surface is the sum of contributions from the radiation and diffraction

potentials,

$$\widehat{Q} = \widehat{Q}^R + \widehat{Q}^D. \tag{2.6}$$

We express these two contributions as

$$\widehat{Q}^R \equiv -(\mathscr{B} - \mathrm{i}\mathscr{C})\,\widehat{p}_a \quad \text{and} \quad \widehat{Q}^D \equiv \Gamma A_0, \tag{2.7}$$

where $\mathscr{B}$ and $\mathscr{C}$ are real and A_0 is the incident wave amplitude. Physically $\mathscr{C}$ is in phase with the flux acceleration and amounts to the added hydrodynamic inertia (i.e. the radiation susceptance). On the other hand, $\mathscr{B}$ is in phase with the flux velocity amounting to radiation damping (i.e. radiation conductance). The quantities $\mathscr{B}$ and $\mathscr{C}$ and the complex response function Γ will be computed in later sections. Combining (2.4) and (2.7), we obtain

$$\frac{\widehat{p}_a}{A_0} = \frac{\Gamma}{\left[\left(\dfrac{KD}{N\rho_a^0} + \mathscr{B}\right) - \mathrm{i}\left(\mathscr{C} + \dfrac{\omega V_o}{c_a^2\rho_a^0}\right)\right]}. \tag{2.8}$$

The power output is the time-averaged rate of work done by the chamber pressure pushing air through the turbine:

$$P_{out} = \overline{\frac{\mathrm{d}(\rho_a V)}{\mathrm{d}t}\frac{p_a}{\rho_a^0}} = \frac{KD}{2N\rho_a^0}\,|\widehat{p}_a|^2 = \frac{KD}{2N\rho_a^0}\,\frac{|\Gamma|^2 A_0^2}{\left(\dfrac{KD}{N\rho_a^0} + \mathscr{B}\right)^2 + \left(\mathscr{C} + \dfrac{\omega V_o}{c_a^2\rho_a^0}\right)^2}. \tag{2.9}$$

In terms of the dimensionless coefficients

$$\widetilde{\Gamma} = \Gamma/\left(\frac{ag}{\omega}\right), \quad (\widetilde{\mathscr{B}}, \widetilde{\mathscr{C}}) = (\mathscr{B}, \mathscr{C})/\left(\frac{a}{\omega\rho_w}\right) \tag{2.10}$$

and

$$\chi = \frac{\rho_w KD\omega}{\rho_a Na}, \quad \beta = \frac{\omega^2 V_o \rho_w}{c_a^2 a \rho_a} \tag{2.11}$$

the efficiency of power extraction can be measured by the capture length L defined by the ratio of power output to the density of power flux of the incident wavefront,

$$kL = \frac{kP_{out}}{\rho g A_0^2 C_g/2} = \frac{gka}{\omega C_g}\,\frac{\chi|\widetilde{\Gamma}|^2}{\left(\chi + \widetilde{\mathscr{B}}\right)^2 + \left(\widetilde{\mathscr{C}} + \beta\right)^2}. \tag{2.12}$$

While the parameter χ characterizes the turbines, β represents the effect of compressibility of air in the chamber and is analogous to a spring constant. As noted by Sarmento & Falcão (1985), this effect of compressibility is mathematically equivalent to adding an imaginary part to the turbine coefficient K and amounts to a phase difference between the mass flow rate and the pressure. As an estimate we take $\omega = 0.5$ rad s^{-1}, $a = 10$ m, $V_o = 10^3$ m^3 and $\rho_w/\rho_a = 10^3$. Then $\beta = 0.43$ which is of the order of unity, indicating the importance of air compressibility.

To obtain the parameters $\widetilde{\mathscr{B}}$, $\widetilde{\mathscr{C}}$ and $\widetilde{\Gamma}$, it is necessary to solve the radiation and diffraction problems. The former is the response to pressure-forced oscillaton of the water surface inside the column. The latter is due to scattering of an incident wave when the water surface everywhere is uniformly atmospheric. The two problems are coupled by the power takeoff relation (2.4). Linearized approximation for small-amplitude waves is used throughout.

3. Diffraction problem

Let the incident wave arrive from the direction $\theta = \alpha$ with respect the breakwater (see figure 1). The diffraction potential is governed by

$$\nabla^2 \varphi = 0, \quad \text{in water,} \tag{3.1}$$

and the boundary conditions

$$\frac{\partial \varphi}{\partial z} - \frac{\omega^2}{g}\varphi = 0, \quad \text{on the water surface } z = 0, \tag{3.2}$$

$$\frac{\partial \varphi}{\partial n} = 0 \quad \text{on all solid boundaries.} \tag{3.3}$$

As is known from past theories the solution can be constructed with the help of the vertical eigenfunctions $Z_0(z)$ and $Z_\ell(z)$, $\ell = 1, 2, 3, \ldots$, defined by

$$Z_0(z) = \frac{\cosh k(z+h)}{N_0^{1/2}}, \quad N_0 = \frac{1}{2}\left[1 + \frac{\sinh 2kh}{2kh}\right], \tag{3.4}$$

where k is the positive real root of the dispersion relation

$$\omega^2 = gk \tanh kh \tag{3.5}$$

and

$$Z_\ell(z) = \frac{\cos \kappa_\ell(z+h)}{N_\ell^{1/2}}, \quad N_\ell = \frac{1}{2}\left[1 + \frac{\sin 2\kappa_\ell h}{2\kappa_\ell h}\right], \quad \ell = 1, 2, 3, \ldots, \tag{3.6}$$

where κ_ℓ, $\ell = 1, 2, 3, \ldots$, are the positive imaginary roots of (3.5), i.e.

$$-\omega^2 = g\kappa_\ell \tan \kappa_\ell h, \quad \ell = 1, 2, 3, \ldots. \tag{3.7}$$

The eigenfunctions $Z_0(z)$ and Z_ℓ, $\ell = 1, 2, 3, \ldots$, satisfy (3.2) as well as the no-flux boundary condition at the sea bottom. Together they form a complete orthogonal set in $-h < z < 0$:

$$\int_{-h}^{0} Z_\ell(z) Z_m(z)\, \mathrm{d}z = h\delta_{\ell m}, \quad \ell, m = 0, 1, 2, 3, \ldots. \tag{3.8}$$

For brevity we shall define $k = \mathrm{i}\kappa_0$ and include $Z_0(z)$ as a member of the complete set of (3.6) with $\ell = 0$.

Let us first represent the total diffraction potential outside the cylinder as the sum of two parts:

$$\varphi_O(r, \theta, z) = \varphi_1 + \varphi_2, \tag{3.9}$$

where φ_1 is due to scattering by a solid cylinder extending the entire sea depth and connected to the breakwater and φ_2 is the correction for the opening. The first part is solved exactly in Appendix A by extending the two-dimensional solution of the classical problem of a vertical wedge by Stoker (1958), with the following result:

$$\varphi_1 = \frac{-\mathrm{i}gA_0}{\omega} \sum_{n=0}^{\infty} \epsilon_n \frac{\cos \dfrac{n\alpha}{2} \mathrm{e}^{-\mathrm{i}n\pi/4} \mathrm{i} Y'_{n/2}(ka)}{H'_{n/2}(ka)} \left[J_{n/2}(kr) - \frac{J'_{n/2}(ka)}{Y'_{n/2}(ka)} Y_{n/2}(kr)\right] \cos\left(\frac{n\theta}{2}\right) \frac{Z_0(z)}{Z_0(0)}, \tag{3.10}$$

where $J_{n/2}$ and $Y_{n/2}$ are the standard Bessel functions of the order of $n/2$. The second part φ_2 is the response to the oscillating pressure associated with φ_1 at the opening $r=a$, $0<\theta<2\pi$, $-h<z<-d$, and is formally expressed as

$$\varphi_2 = \frac{-\mathrm{i}gA_0}{\omega}\sum_{\ell=0}^{\infty} Z_\ell(z)\sum_{n=0}^{\infty} A_{n\ell}\frac{K_{n/2}(\kappa_\ell r)}{\kappa_\ell a\ K'_{n/2}(\kappa_\ell a)}\cos\frac{n\theta}{2} \tag{3.11}$$

which satisfies the no-flux condition on both sides of the breakwater ($\theta=0,\ 2\pi$); $K_{n/2}$ denotes the modified Bessel function of the second kind of the order of $n/2$. The coefficients $A_{n\ell}$ are yet unknown. Note that the terms with $\ell=0$ correspond to an outgoing wave

$$K_{n/2}(-\mathrm{i}kr) = \frac{\pi}{2}\mathrm{i}^{(n/2)+1}H^{(1)}_{n/2}(kr). \tag{3.12}$$

The potential inside the cylinder $r<a$, $0<\theta<2\pi$ is due entirely to the opening

$$\varphi_C = \frac{-\mathrm{i}gA_0}{\omega}\sum_{n=0}^{\infty}\sum_{\ell=0}^{\infty}(B_{n\ell}\cos n\theta + C_{n\ell}\sin n\theta)\frac{I_n(\kappa_\ell r)}{\kappa_\ell a\ I'_n(\kappa_\ell a)}Z_\ell(z), \tag{3.13}$$

where $B_{n\ell}$ and $C_{n\ell}$ are also unknown. Note that for $\ell=0$, $\kappa_0=-\mathrm{i}k$ and

$$I_{n/2}(-\mathrm{i}kr) = (-\mathrm{i})^{n/2}J_{n/2}(kr). \tag{3.14}$$

Since φ_1 already satisfies the no-flux condition on the cylindrical surface $r=a$ for the entire water depth, φ_2 and φ_C must satisfy

$$\frac{\partial\varphi_2}{\partial r} = \frac{\partial\varphi_C}{\partial r} = \begin{cases} 0, & -d<z<0, \\ U(z,\theta), & -h<z<-d, \end{cases} \qquad 0<\theta<2\pi, \tag{3.15}$$

which implies

$$\begin{aligned}\sum_{n=0}^{\infty}\sum_{\ell=0}^{\infty}A_{n\ell}\cos\frac{n\theta}{2}Z_\ell(z) &= \sum_{n=0}^{\infty}\sum_{\ell=0}^{\infty}(B_{n\ell}\cos n\theta + C_{n\ell}\sin n\theta)\,Z_\ell(z) \\ &= \begin{cases} 0, & -d<z<0, \\ \dfrac{\mathrm{i}a\omega}{gA_0}U(z,\theta), & -h<z<-d, \end{cases} \qquad 0<\theta<2\pi. \end{aligned} \tag{3.16}$$

Using orthogonality, we get for any integer ℓ and n

$$\frac{2\pi}{\epsilon_n}A_{n,\ell} = \frac{\mathrm{i}a\omega}{ghA_0}\int_0^{2\pi}\int_{-h}^{-d}U(\theta,z)Z_\ell(z)\cos\frac{n\theta}{2}\mathrm{d}\theta\mathrm{d}z, \tag{3.17}$$

$$\frac{2\pi}{\epsilon_n}\{B_{n,\ell}\ ;\ C_{n,\ell}\} = \frac{\mathrm{i}a\omega}{ghA_0}\int_0^{2\pi}\int_{-h}^{-d}U(\theta,z)Z_\ell(z)\{\cos(n\theta)\ ;\ \sin(n\theta)\}\mathrm{d}\theta\mathrm{d}z. \tag{3.18}$$

Since the pressure must also be continuous at the opening, we require

$$\varphi_1+\varphi_2=\varphi_C, \qquad r=a, -h<z<-d \tag{3.19}$$

so that

$$\begin{aligned}\sum_{n=0}^{\infty}\left[\mathscr{E}_n\cos\frac{n\theta}{2}Z_0(z) + \sum_{\ell=0}^{\infty}A_{n\ell}\frac{K_{n/2}(\kappa_\ell a)}{\kappa_\ell a\ K'_{n/2}(\kappa_\ell a)}\cos\frac{n\theta}{2}Z_\ell(z)\right] \\ = \sum_{n=0}^{\infty}\sum_{\ell=0}^{\infty}(B_{n\ell}\cos n\theta + C_{n\ell}\sin n\theta)\frac{I_n(\kappa_\ell a)}{\kappa_\ell a\ I'_n(\kappa_\ell a)}Z_\ell(z), \end{aligned} \tag{3.20}$$

where

$$\mathscr{E}_n = \epsilon_n \frac{\cos\dfrac{n\alpha}{2} \mathrm{e}^{-\mathrm{i}n\pi/4} \mathrm{i} Y'_{n/2}(ka)}{Z_0(0) H'_{n/2}(ka)} \left(J_{n/2}(ka) - \frac{J'_{n/2}(ka)}{Y'_{n/2}(ka)} Y_{n/2}(ka) \right) \tag{3.21}$$

is associated with φ_1. After using (3.17) and (3.18), an integral equation for $U(\theta, z)$ is obtained,

$$\int_0^{2\pi} \int_{-h}^{0} \mathrm{d}\theta' \mathrm{d}z' \; U(z', \theta') \; \mathscr{K}(z, \theta; z', z', \theta') = \frac{-2\pi \mathrm{i} g A_0}{a\omega} \sum_{n=0}^{\infty} \mathscr{E}_n \cos\frac{n\theta}{2} Z_0(z),$$
$$0 < \theta < 2\pi, \quad -h < z < -d, \tag{3.22}$$

with the kernel

$$\begin{aligned} &\mathscr{K}(z, \theta; z', \theta' \\ &\quad \equiv \sum_{n=0}^{\infty} \sum_{\ell=0}^{\infty} \frac{\epsilon_n}{h} \frac{I_n(\kappa_\ell a)}{\kappa_\ell a \; I'_n(\kappa_\ell a)} Z_\ell(z) Z_\ell(z') [\sin(n\theta) \sin(n\theta') + \cos(n\theta) \cos(n\theta')] \\ &\quad - \sum_{n=0}^{\infty} \sum_{\ell=0}^{\infty} \frac{\epsilon_n}{h} \frac{K_{n/2}(\kappa_\ell a)}{\kappa_\ell a \; K'_{n/2}(\kappa_\ell a)} Z_\ell(z) Z_\ell(z') \cos\left(\frac{n\theta}{2}\right) \cos\left(\frac{n\theta'}{2}\right). \end{aligned} \tag{3.23}$$

The integral equation is solved by an efficient method due to Evans & Porter (1997) for a similar problem in two dimensions. Let $U(\theta, z)$ be expanded as

$$U(\theta, z) = \frac{-\mathrm{i} g A_0}{\omega} \sum_{m=0}^{\infty} \sum_{p=0}^{\infty} (\alpha_{mp} \cos m\theta + \beta_{mp} \sin m\theta) u_p(z) \tag{3.24}$$

with

$$u_n(z) = \frac{2(-1)^n}{\pi \sqrt{(h-d)^2 - (z+h)^2}} T_{2n}\left(\frac{z+h}{h-d}\right), \tag{3.25}$$

where T_n is the Chebychev polynomials of the order of n. Making use of the identity (Erdélyi, Magnus & Tricomi 1954)

$$F_{n\ell} \equiv \int_{-h}^{-d} u_n(z) Z_\ell(z) \mathrm{d}z = N_\ell^{-1/2} J_{2n}\{\kappa_\ell(h-d)\}, \tag{3.26}$$

where N_ℓ is the normalization coefficient defined in (3.6), the integral equation (3.22) may be written as

$$\begin{aligned} &\sum_{n=0}^{\infty} 2\pi \frac{h}{a} \mathscr{E}_n \cos\frac{n\theta}{2} Z_0(z) \\ &\quad = -\sum_{n=0}^{\infty} \sum_{\ell=0}^{\infty} \sum_{m=0}^{\infty} \sum_{p=0}^{\infty} \epsilon_n \beta_{mp} F_{p\ell} \frac{4m(1-(-1)^n)}{4m^2 - n^2} \frac{K_{n/2}(\kappa_\ell a)}{\kappa_\ell a \; K'_{n/2}(\kappa_\ell a)} \cos\frac{n\theta}{2} Z_\ell(z) \\ &\qquad - \sum_{n=0}^{\infty} \sum_{\ell=0}^{\infty} \sum_{m=0}^{\infty} \sum_{p=0}^{\infty} 2\pi \alpha_{mp} F_{p\ell} \delta_{(n/2)m} \frac{K_{\frac{n}{2}}(\kappa_\ell a)}{\kappa_\ell a \; K'_{n/2}(\kappa_\ell a)} \cos\frac{n\theta}{2} Z_\ell(z) \\ &\qquad + \sum_{n=0}^{\infty} \sum_{\ell=0}^{\infty} \sum_{m=0}^{\infty} \sum_{p=0}^{\infty} 2\pi \beta_{mp} F_{p\ell} \delta_{nm} (1 - \delta_{n0}) \frac{I_n(\kappa_\ell a)}{\kappa_\ell a \; I'_n(\kappa_\ell a)} \sin n\theta \, Z_\ell(z) \\ &\qquad + \sum_{n=0}^{\infty} \sum_{\ell=0}^{\infty} \sum_{m=0}^{\infty} \sum_{p=0}^{\infty} 2\pi \alpha_{mp} F_{p\ell} \delta_{nm} \frac{I_n(\kappa_\ell a)}{\kappa_\ell a \; I'_n(\kappa_\ell a)} \cos n\theta \, Z_\ell(z). \end{aligned} \tag{3.27}$$

Multiplying (3.27) by $u_{p'}(z)\cos(m'\theta)$ and $u_{p'}(z)\sin(m'\theta)$ in turn, integrating over the range $0 < \theta < 2\pi$, $-h < z < -d$ and using (3.26), we get for any p' and m' two algebraic systems for the coefficients α_{mp} and β_{mp}:

$$\mathscr{E}_{2m'} F_{p'0} \frac{h}{a} = \sum_{m=0}^{\infty}\sum_{p=0}^{\infty} \alpha_{mp} \left\{ \delta_{mm'} \sum_{\ell=0}^{\infty} \left[\frac{I_{m'}(\kappa_\ell a)}{\kappa_\ell a \; I'_{m'}(\kappa_\ell a)} - \frac{K_{m'}(\kappa_\ell a)}{\kappa_\ell a \; K'_{m'}(\kappa_\ell a)} \right] F_{p\ell} F_{p'\ell} \right\} \tag{3.28}$$

and

$$\sum_{n=0}^{\infty} 2\pi \frac{h}{a} \mathscr{E}_n F_{p'0} \frac{4m'(1-(-1)^n)}{4m'^2 - n^2}$$
$$= \sum_{m=0}^{\infty}\sum_{p=0}^{\infty} \beta_{mp} \left\{ 2\pi^2 \delta_{mm'} \sum_{\ell=0}^{\infty} \frac{I_{m'}(\kappa_\ell a)}{\kappa_\ell a \; I'_{m'}(\kappa_\ell a)} F_{p\ell} F_{p'\ell} \right\} - \sum_{m=0}^{\infty}\sum_{p=0}^{\infty}$$
$$\times \beta_{mp} \left\{ \sum_{n=0}^{\infty}\sum_{\ell=0}^{\infty} \epsilon_n \frac{K_{n/2}(\kappa_\ell a)}{\kappa_\ell a \; K'_{n/2}(\kappa_\ell a)} F_{p\ell} F_{p'\ell} \frac{16mm'(1-(-1)^n)^2}{(4m^2 - n^2)(4m'^2 - n^2)} \right\}. \tag{3.29}$$

The infinite series are truncated. Let the upper limit of the m-series of sines/cosines be M and the upper limit of vertical eigenmodes and Chebychev polynomials p be P. We first convert the two-dimensional matrices as vectors:

$$\{\alpha\} = \{\alpha_{00},\ \alpha_{01},\ \ldots,\ \alpha_{0P},\ \alpha_{10},\ \alpha_{11},\ \ldots,\ \alpha_{1P},\ \ldots\ \ldots,\ \alpha_{M0},\ \alpha_{M1},\ \ldots,\ \alpha_{MP}\}, \tag{3.30}$$

$$\{\beta\} = \{\beta_{10},\ \beta_{11},\ \ldots,\ \beta_{1P},\ \beta_{20},\ \beta_{21},\ \ldots,\ \beta_{2P},\ \ldots\ \ldots,\ \beta_{M0},\ \beta_{M1},\ \ldots,\ \beta_{MP}\}. \tag{3.31}$$

Thus, $\alpha_{mp} = \alpha_k$ with $k = m \cdot (P+1) + p$, and the systems to be numerically solved are

$$\sum_{k=0}^{(M+1)(P+1)} K^e_{k'k} \alpha_k = V^e_{k'} \qquad \sum_{k=P+1}^{(M+1)(P+1)} K^o_{k'k} \beta_k = V^o_{k'}; \quad k' = 0, 1, \ldots, (M+1)(P+1), \tag{3.32}$$

where

$$K^e_{k'k} = \delta_{mm'} \sum_{\ell=0}^{P} \left[\frac{I_{m'}(\kappa_\ell a)}{\kappa_\ell a \; I'_{m'}(\kappa_\ell a)} - \frac{K_{m'}(\kappa_\ell a)}{\kappa_\ell a \; K'_{m'}(\kappa_\ell a)} \right] F_{p\ell} F_{p'\ell},$$

$$V^e_{k'} = \mathscr{E}_{2m'} F_{p'0} \frac{h}{a}, \qquad V^o_{k'} = \sum_{n=0}^{M} 2\pi \frac{h}{a} \mathscr{E}_n F_{p'0} \frac{4m'(1-(-1)^n)}{4m'^2 - n^2},$$

$$K^o_{k'k} = 2\pi^2 \delta_{mm'} \sum_{\ell=0}^{P} \frac{I_{m'}(\kappa_\ell a)}{\kappa_\ell a \; I'_{m'}(\kappa_\ell a)} F_{p\ell} F_{p'\ell}$$
$$- \sum_{n=0}^{M}\sum_{\ell=0}^{P} \epsilon_n \frac{K_{n/2}(\kappa_\ell a)}{\kappa_\ell a \; K'_{n/2}(\kappa_\ell a)} F_{p\ell} F_{p'\ell} \frac{16mm'(1-(-1)^n)^2}{(4m^2 - n^2)(4m'^2 - n^2)}, \tag{3.33}$$

with the convention $m = \lfloor k/(P+1) \rfloor$ and $p = k - (P+1)\lfloor k/(P+1) \rfloor$ and similar notations for primed indices.

After solving the truncated systems numerically, all the coefficients $A_{n\ell}$, $B_{n\ell}$ and $C_{n\ell}$ can be computed from (3.17) and (3.18). Then the diffraction potential in the entire fluid is found. In particular, we get from (3.13)

$$\Gamma = \frac{1}{A_0}\int_0^a r\,\mathrm{d}r \int_0^{2\pi} \mathrm{d}\theta \frac{\partial \phi_C}{\partial z}|_{z=0} = \frac{-2\pi \mathrm{i} g}{\omega}\int_0^a \sum_{\ell=0}^{\infty} B_{0\ell}\frac{I_n(\kappa_\ell r)}{\kappa_\ell a\ I_n'(\kappa_\ell a)} Z_\ell'(0) r\,\mathrm{d}r. \qquad (3.34)$$

In addition to checking with the limiting cases of a semi-infinite breakwater without the cylinder, checking is also performed with an isolated vertical cylinder. Correctness and accuracy of our computations have been validated by comparing our results for head-sea incidence ($\alpha = \pi$) with Garrett (1970) for a bottomless harbour in an open sea. When $\alpha = \pi$, all terms of odd n disappear in the series of (3.10) which is the solution for the isolated cylinder in the open sea. Physically the thin breakwater is virtually absent. We have also checked an identity which relates Γ and the radiation damping rate $\mathscr{B}$ (Evans 1982) as will be discussed in the next section. In all cases, the agreement is excellent, and the plotted results cannot be distinguished.

Sample numerical results are displayed in figure 2 for the free surface inside and outside the cylinder at the lowest resonance frequency. The dimensions are chosen to be typical for an OWC design with $a/h = 0.5$ and $d/h = 0.2$. Note that the free surface inside is roughly uniform and insensitive to the angle of incidence α. However, the free surface outside depends strongly on α. The free-surface amplitude along the outside wall of the cylinder is also shown in figure 3 for $ka \approx 1$. These results are useful for computing wave forces on the structure. Generally, the elevation on the incidence side along the breakwater ($\theta \sim 0$) is significantly larger than that on an isolated cylinder. On the shadow side the elevation is considerably reduced as expected. To see the effects of the opening, the results for a solid cylinder without opening are also shown. The pressure on the exposed side is lessened, while that on the shadow side is increased. The difference between the solid and open cylinders is very significant for relatively long waves ($ka \approx 1$ here). For shorter wave, e.g. $ka \approx 3$, waves outside do not penetrate the opening, and the difference is small.

In early computations it was noted that the vertical flux rate due to the fluctuating water surface in the column, i.e. Γ, is independent of the angle of incidence α. This surprising result can be proven as follows: By mass conservation, the said vertical flux is equal to the total radial flux (the area integral of $U(\theta, z)$) through the submerged opening. As seen from (3.24), this radial flux depends only on the coefficients α_{0p}, $p = 0, 1, 2, 3, \ldots$, which in turn depends only on $\mathscr{E}_0$ as can be seen from (3.28). However by definition (3.21), $\mathscr{E}_0$ corresponds to the isotropic term of the diffraction problem φ_1 and is independent of the angle of incidence. It follows that both the radial flux and Γ are also independent of α. It was remarked by Professor A. Falcão that if a circular buoy heaves inside the column, this independence should also hold as long as the buoy is axially symmetric.

Since the radiation problem is axially symmetric, coefficients $\mathscr{B}$ and $\mathscr{C}$ are independent of the incidence angle as well. It follows from (2.9) that the power output is the same for all incidence angles, despite the presence of the breakwater. Since in the special case $\alpha = \pi$, the breakwater is ineffective, power absorption here is the same as if the OWC unit were in the open sea. Thus the existence of the breakwater affects only the wave patterns outside and inside, hence the wave forces on the structure, but not the averaged vertical flux inside the OWC.

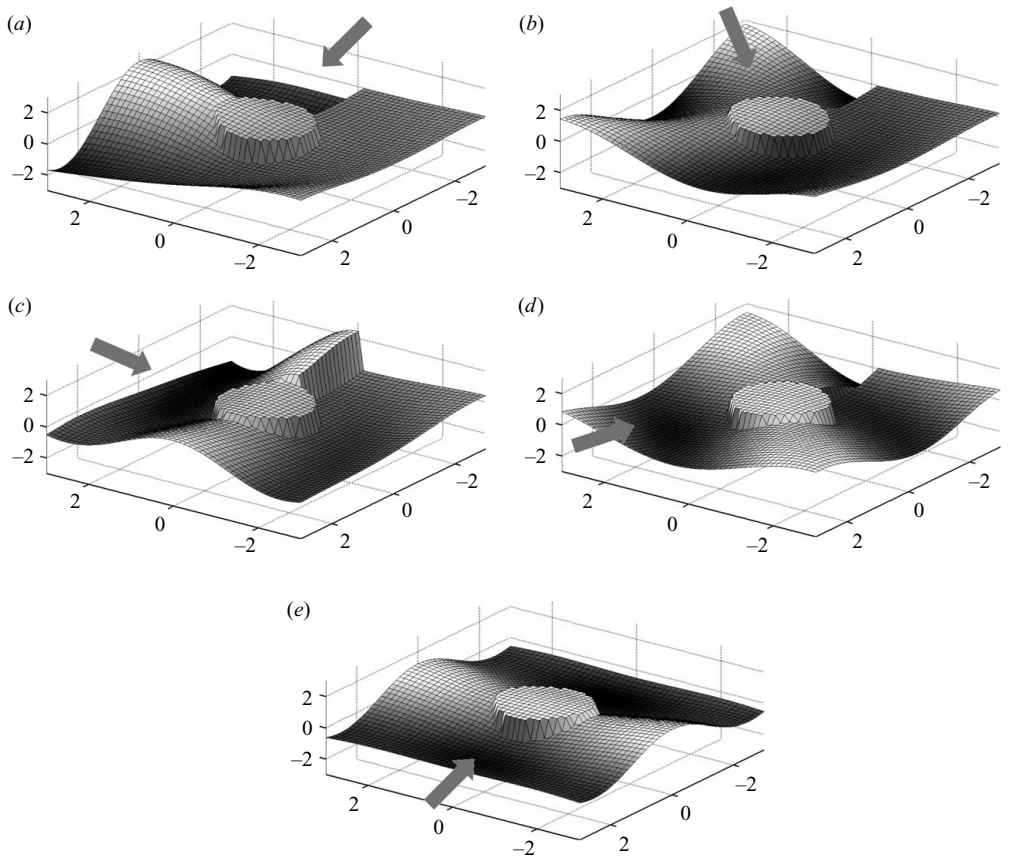

FIGURE 2. Free-surface elevation inside and around the cylinder for different incidence angles at the lowest resonance frequency: $a/h = 0.5$; $d/h = 0.2$; $ka = 1.27$; $t = 0$. From top left to bottom, as α increases: (*a*) tail-sea incidence $\alpha = 0$; (*b*) oblique incidence $\alpha = \pi/4$; (*c*) normal incidence $\alpha = \pi/2$; (*d*) oblique incidence $\alpha = 3\pi/4$; (*e*) head-sea incidence $\alpha = \pi$.

Of course any deviation from the simple geometry, such as finite thickness of the breakwater and absence of axisymmetry of the submerged opening, should destroy this independence.

4. Radiation problem

Since the air pressure is assumed to be spatially uniform, the radiation problem is axially symmetric; the thin breakwater has no effect. The radiation problem is the same as that studied by Evans & Porter (1997) for a circular OWC in the open sea. We have repeated their calculations to obtain all the hydrodynamic coefficients.

For evaluating the energy extracted, the coefficients $\widetilde{\mathscr{B}}$ and $\widetilde{\mathscr{C}}$ are calculated from (2.7) after normalization according to (2.10), as shown in figure 4 for one draft and different radii. It is worth noting that the radiation damping and the diffraction-induced vertical flux in the column are linked through an identity due to Evans (1982):

$$B = \frac{k}{8\pi\rho g A_0^2 C_g} \int_0^{2\pi} |\widehat{Q}^D(\alpha)|^2 \mathrm{d}\alpha. \tag{4.1}$$

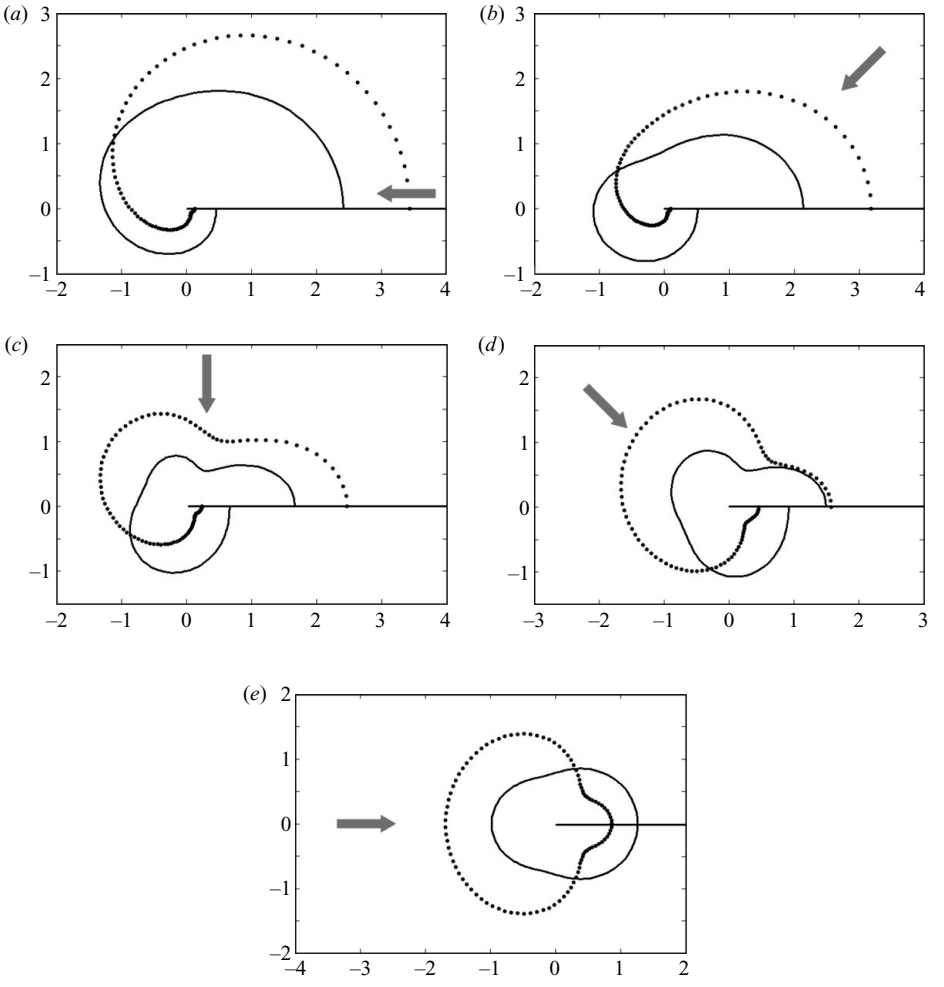

FIGURE 3. Polar plot of the free-surface elevation amplitude along the outside wall of the cylinder, $r = a$, for different incidence angles, $a/h = 0.5$; $ka = 1.12$. Dots: cylinder extending to the bottom. Solid line: truncated empty cylinder with $d/h = 0.2$. From top left to bottom, as α increases: (a) tail-sea incidence $\alpha = 0$; (b) oblique incidence $\alpha = \pi/4$; (c) normal incidence $\alpha = \pi/2$; (d) oblique incidence $\alpha = 3\pi/4$; (e) head-sea incidence $\alpha = \pi$.

As was just proven $\widehat{Q}^D \propto \Gamma$ is independent of α; hence the above identity reduces to

$$B = \frac{k\left|\widehat{Q}^D\right|^2}{4\rho g A_0^2 C_g}, \qquad \text{i.e.} \qquad \widetilde{B} = \frac{kag\left|\widetilde{\Gamma}\right|^2}{4C_g\omega}. \tag{4.2}$$

This relation has been used as another check for the accuracy of separate computations of radiation and diffraction potentials. For the present geometry, a mathematical consequence of (4.2) is that if only the extracted power is required, there is no need to solve the diffraction problem, since $|\Gamma|$ can be deduced directly from $\mathscr{B}$ which is the result of the simpler radiation problem. Of course this shortcut is hard to recognize in advance of our proof.

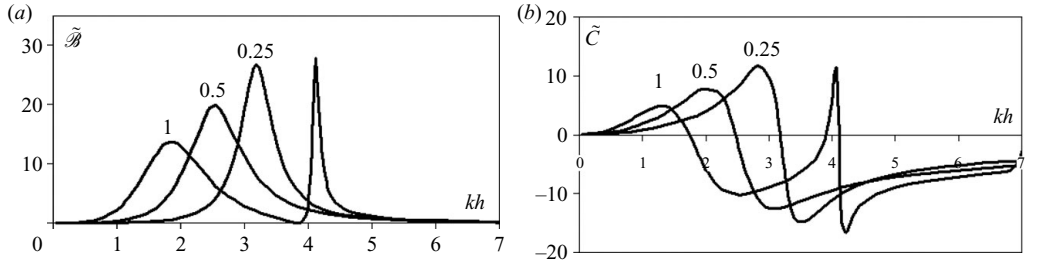

FIGURE 4. (*a*) Radiation damping and (*b*) added mass coefficients as functions of the normalized frequency kh for $a/h = 0.25,\ 0.5,\ 1$. In all cases $d/h = 0.2$.

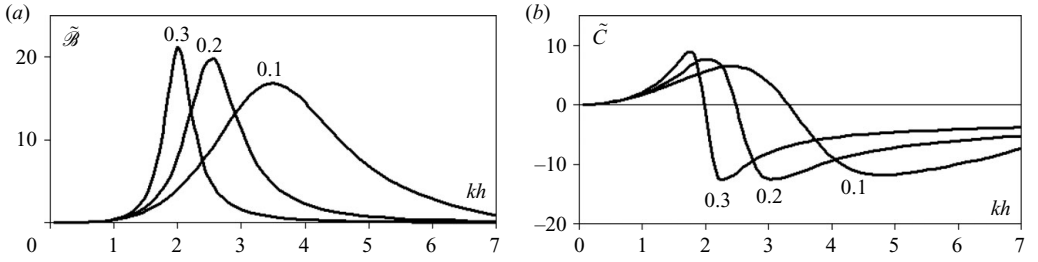

FIGURE 5. (*a*) Radiation damping and (*b*) added mass coefficients as functions of the normalized frequency kh for $d/h = 0.1,\ 0.2,\ 0.3$. In all cases $a/h = 0.5$.

As can be seen in figure 4, for relatively small columns ($a/h = 0.25, 0.5$), the damping is positive in the computed range of kh. For the larger column $a/h = 1$, $\widetilde{\mathscr{B}}$ vanishes at $kh = 3.83$ which corresponds to the smallest zero of $J_0'(ka)$ when there is no radiation due to destructive interference, i.e. $\widetilde{\mathscr{B}} = 0$ (The first three zeros of $J_0'(ka)$ are at $ka = 3.83, 7.02, 10.17$). This zero is known to exist from the two-dimensional theory of waves created by a finite band of uniform surface pressure (Stoker 1958) and can be easily derived for three dimensions with a uniform pressure in a circle. Note also that, unlike the case of a rigid floating body, the added mass $\widetilde{\mathscr{C}}$ changes sign and is shaped like the letter N. For $a/h = 0.25, 0.5$ there is only one N; for $a/h = 1$ there are two, separated by the zero of $J'(ka)$. This characteristic is known in two- and three-dimensional OWC systems (Smith 1983; Sarmento & Falcão 1985; Evans & Porter 1995). Both the frequency and the amplitude of the resonance peak decrease with increasing a/h. On the other hand, a larger radius a leads to a wider bandwidth. Physically, as a/h becomes smaller, the fluid inside the OWC moves like a solid piston. In the limit a hydrostatic approximation predicts resonance at $kd\tanh(kh) = 1$ (which corresponds to $kh \approx 5$). This trend is indeed consistent with the computed results for small radii.

Figure 5 shows the effects of draft d/h for a fixed radius $a/h = 0.5$. Clearly smaller d/h (i.e. larger opening) leads to lower and flatter curves of $\widetilde{\mathscr{B}}$ and $\widetilde{\mathscr{C}}$. It is interesting to note that a larger opening gives a larger frequency bandwidth.

5. Extracted power

We wish to explore how to optimize the power takeoff characteristics and system dimensions with special focus on the effects of air compressibility.

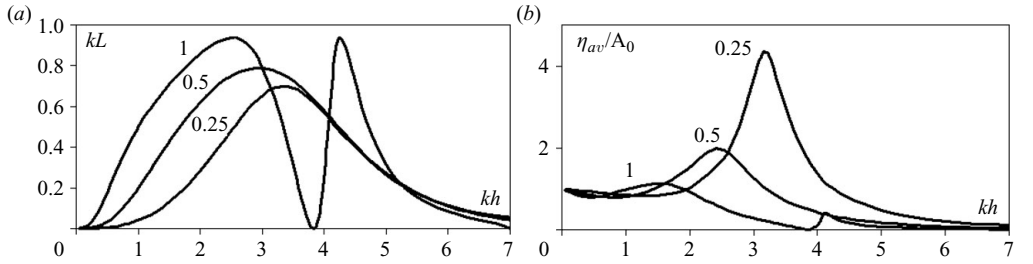

FIGURE 6. (*a*) Capture length and (*b*) average free-surface elevation inside the OWC as functions of the normalized frequency kh for different column sizes a/h. For $d/h = 0.2$, $h = 10$ m, $a/h = 0.25,\ 0.5,\ 1$.

As a preliminary, we choose a sample case in which the sea depth and power takeoff system is similar to those of the pilot station in Pico Island, Azores, Portugal, i.e. $D = 2a$, $V_o = \pi a^2 h$, $N = 2000$ r.p.m., $K = 0.45$ (for one turbine), $h = 10$ m, $\rho_w/\rho_a = 1000$, $g = 9.8\,\mathrm{m\,s^{-2}}$ and $c_a = 340\,\mathrm{m\,s^{-1}}$, and study how the size of the OWC affects the power extraction.

The normalized capture length kL defined in (2.12) is plotted in figure 6. Also shown is the mean water-surface displacement η_{av} inside the column, obtained after calculating the chamber pressure $\hat{p}_a$ and averaged over the cross-section. This averaged displacement is directly proportional to $\mathrm{d}V/\mathrm{d}t = Q$ in (2.2) which is responsible for energy extraction as derived in (2.9). It may also be observed by comparing figure 6 with figure 4 that η_{av} and $\widetilde{\mathscr{B}}$ have roughly the same resonance frequencies at $kh \approx 1.5,\ 2.5,\ 3.2,\ 4.1$. When the cylinder radius is not large, e.g. $a/h \leqslant 0.5$, both kL and η_{av} have only one resonance peak in the computed range of kh, dominated by the Helmholtz mode in which the free surface in the chamber is essentially horizontal. The peak for η_{av} is higher for a smaller cylinder and occurs at a larger kh. But for the larger column with $a/h = 1$ there are two resonance peaks separated by the first zero of $J_0'(ka)$ at $ka = kh = 3.83$. The capture length kL for different column radii also has peaks around the same resonance frequencies. Note that the maximum and the bandwidth of kL increase with the cylinder radius.

In reference to (2.12), the maximum efficiency can be achieved by choosing the turbine characteristics χ and the chamber size, for one frequency only. Let us first optimize the turbines and take $\partial(kL)/\partial\chi = 0$ to get

$$\chi(\omega) = \sqrt{\widetilde{\mathscr{B}(\omega)}^2 + (\widetilde{\mathscr{C}(\omega)} + \beta(\omega))^2}. \tag{5.1}$$

The chamber size and the column geometry are fixed and cannot be easily adjusted. Hence β cannot be optimized for a broad range of ω. If, for any single ω, $\widetilde{\mathscr{C}}(\omega) + \beta(\omega) = 0$, then $\chi(\omega) = \widetilde{\mathscr{B}(\omega)}$; the maximum capture length attainable at that frequency is

$$kL_{max} = \frac{gka}{C_g\omega}\frac{\left|\widetilde{\Gamma}\right|^2}{4\widetilde{B}} = 1. \tag{5.2}$$

The second equality follows from (4.2). It is of course more desirable to strive for high efficiency for a broadband of frequencies. In practice, it is hard to vary the chamber volume (hence β) for different ω but likely more feasible to vary the power

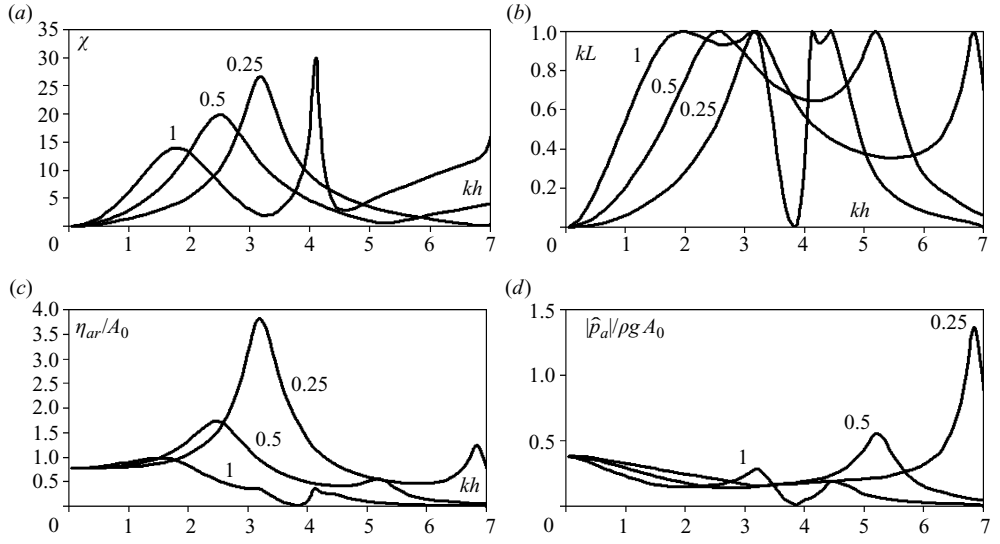

FIGURE 7. Results by optimizing only the turbine characteristics χ over a wide range of kh: (a) optimal turbine parameter; (b) optimal capture width; (c) average free-surface elevation inside the OWC; (d) average pressure inside the OWC; $h = 10$ m, $d/h = 0.2$, $V_o = \pi a^2 h$, $a/h = 0.25,\ 0.5,\ 1$.

takeoff characteristics χ. For example, one can control the turbine constant K by using several turbines and changing the blade angle and rotation speed and the like, for a broad range of frequencies. Let us choose the best χ according to (5.1) over a wide interval of kh under the constraint of fixed chamber volume V_o (or β).

The optimum capture length is then

$$kL_{opt}(\omega) = \frac{4\widetilde{\mathscr{B}}(\omega)\sqrt{\widetilde{\mathscr{B}}(\omega)^2 + (\widetilde{\mathscr{C}}(\omega) + \beta(\omega))^2}}{\left(\sqrt{\widetilde{\mathscr{B}}(\omega)^2 + (\widetilde{\mathscr{C}}(\omega) + \beta(\omega))^2} + \widetilde{\mathscr{B}}(\omega)\right)^2 + (\widetilde{\mathscr{C}}(\omega) + \beta(\omega))^2}. \tag{5.3}$$

The best turbine parameter χ and the resulting kL by this control strategy are shown in figure 7. The corresponding air pressure and η_{av} are also presented as functions of kh for several column sizes: $a/h = 0.25,\ 0.5,\ 1$. There is clearly a qualitative difference from figure 6. In particular the bandwidth of kL is now greater. For the smaller columns, $a/h = 0.25, 0.5$, kL and η_{av} now have two peaks within the computed range of kh. For the large column with $a/h = 1$, there are four peaks in the same range of kh, with two on each side of the the zero of $J_0'(ka)$ at $ka = kh = 3.83$. Note also that the air pressure $\widehat{p}_a$ in the chamber and the turbine parameter χ show only half the number of peaks. For example, for $a/h = 0.5$ the peak of χ is at $kh \approx 2.6$, while the peak of $\widehat{p}_a$ is at $kh \approx 5.2$. The reason is as follows: At these frequencies, (5.1) for χ and (2.8) for $\widehat{p}_a$ can be simplified to $\chi = \widetilde{\mathscr{B}}$ and $\widehat{p}_a \propto 1/\sqrt{\widetilde{\mathscr{B}}}$ by using the fact that $\beta = \widetilde{\mathscr{C}}$. Now, $\widetilde{\mathscr{B}}$ is maximum around the first peak ($kh \approx 2.6$) and very small at the second ($kh \approx 5.2$) as shown in figure 4. Hence χ is small, but $\widehat{p}_a$ is large at $kh \approx 5.2$.

The presence of double peaks has been noted before by Sarmento & Falcão (1985) in their study of a two-dimensional OWC system. Recall that for maximum capture length, $\beta = \widetilde{\mathscr{C}}$, i.e. the curves β versus kh and $\widetilde{\mathscr{C}}$ versus kh must intersect. If the

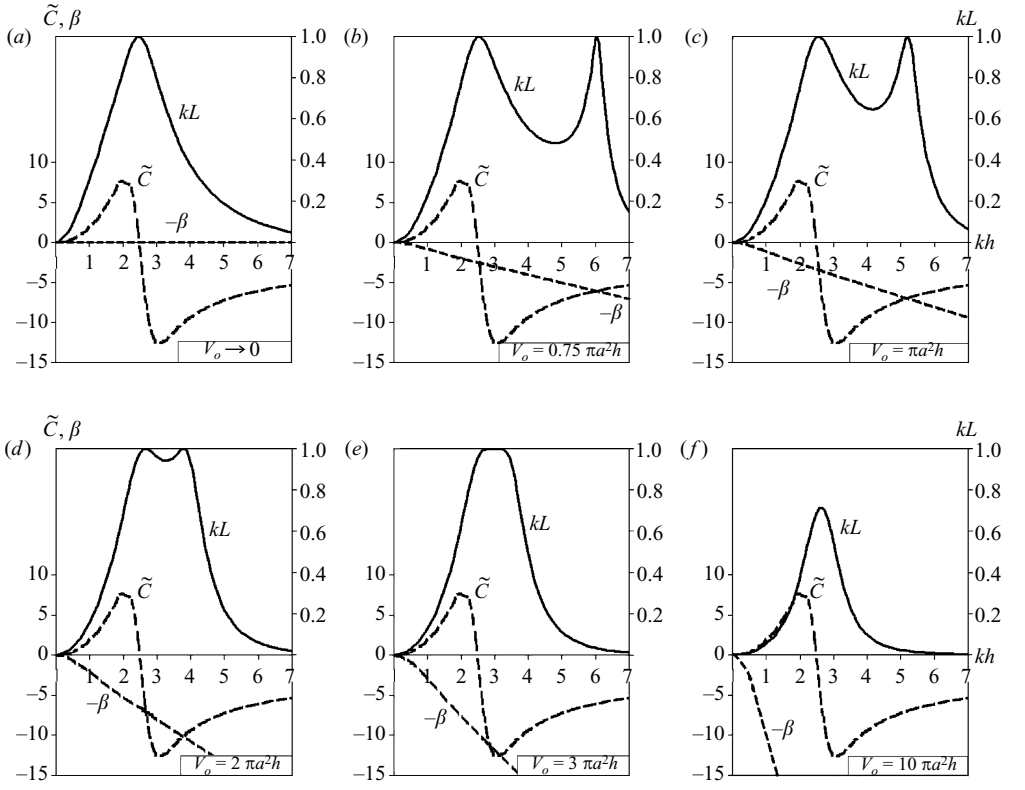

FIGURE 8. Added mass (dashed), β coefficient (dotted) and optimal capture length (solid) as functions of depth-to-wavelength ratio kh, for different pneumatic chamber volumes V_o; $a/h = 0.5$, $d/h = 0.2$, $h = 10$ m: (*a*) $V_o \to 0$ (incompressible case); (*b*) $V_o = 0.75\pi a^2 h$; (*c*) $V_o = \pi a^2 h$; (*d*) $V_o = 2\pi a^2 h$; (*e*) $V_o = 3\pi a^2 h$; (*f*) $V_o = 10\pi a^2 h$.

curve of $\widetilde{\mathscr{C}}$ is shaped as a single N such as figure 4 for $a/h = 0.25, 0.5$, there can be two points of intersection, hence two peaks of kL. In figure 8 we consider different values of β by increasing the chamber volume V_o. If $V_o = 0$ or, equivalently, if air compressibility is ignored, $\beta = 0$, and there is only one intersection at $\widetilde{C} = 0$ resulting in just one maximum efficiency. We note that $\beta \propto \omega^2 \propto kh \tanh(kh)$ so that β is almost linear in kh for sufficiently short waves. As V_o increases, the β curve is inclined downward, causing two intersection points, hence two maxima and wider bandwidth in efficiency. Further increase of V_o brings the two intersecting points together. If V_o exceeds a certain limit, there is no intersection, and the optimum efficiency, $kL = 1$, cannot be achieved. For any a, d and h there is only a finite range of V_o in which kL is optimum for two different frequencies.

For a relatively large column with $a/h = 1$, the $\widetilde{\mathscr{C}}$ curve consists of two N, as is shown in figure 9. Hence there are four peaks of kL, and the efficiency is high for a much greater bandwidth.

In short we can thank compressibility of air in the chamber for broadening the bandwidth of the extraction efficiency.

Finally we display the effects of the draft d/h in figure 10; kL, η_{av}, the pressure and the optimum χ are shown for different values of cylinder draft $d/h = 0.1,\ 0.2,\ 0.3$. It can be seen that a smaller draft leads to a better efficiency (bandwidth and amplitude)

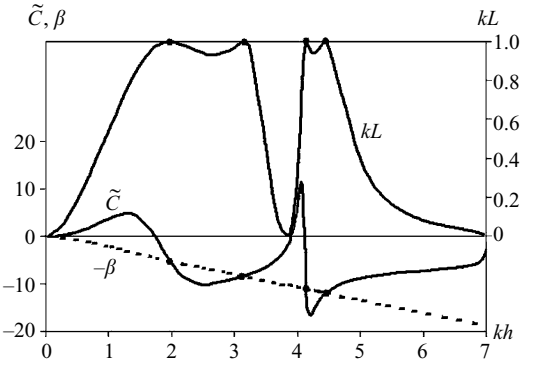

FIGURE 9. Relation between the optimal capture length and the variations of β and added mass coefficient $\widetilde{\mathscr{C}}$ for a large column with $a/h = 1$ and draft $d/h = 0.2$; $V_o = \pi a^2 h$, $h = 10$ m.

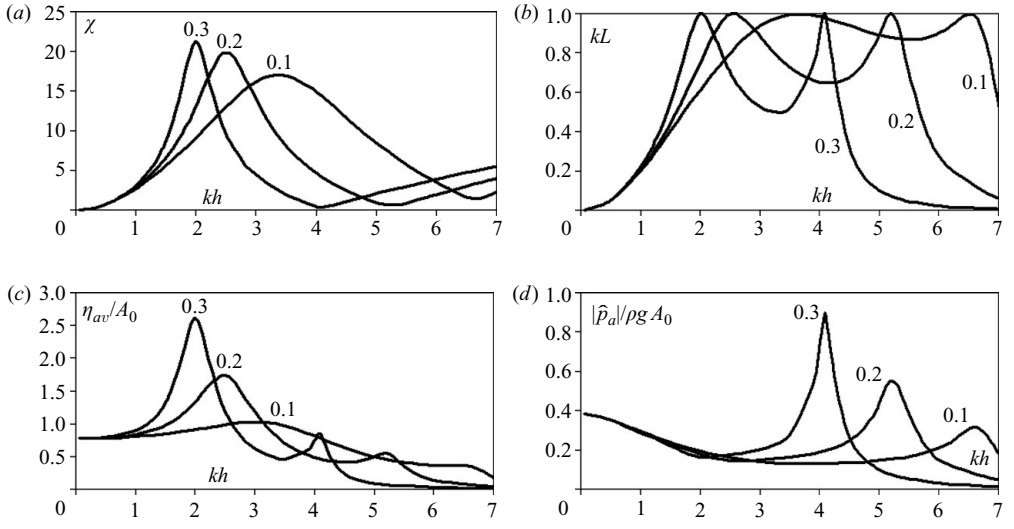

FIGURE 10. (*a*) Optimal turbine parameter χ; (*b*) capture length; (*c*) average free-surface elevation inside the chamber; (*d*) average chamber pressure; $a/h = 0.5$, $V_o = \pi a^2 h$, $h = 10$ m, $d/h = 0.1,\ 0.2,\ 0.3$.

for this particular choice of chamber volume. Resonance occurs at higher frequencies if the draft is smaller. Recall that as the draft decreases, the curve of $\widetilde{\mathscr{C}}(kh)$ becomes flatter. Thus the two intersection points between the $-\beta(kh)$ and $\widetilde{\mathscr{C}}(kh)$ curve are wider apart. This explains why the smaller draft corresponds to a broader efficiency bandwidth. In practice the draft must be deep enough so that air cannot penetrate the chamber for large-amplitude waves.

6. Concluding remarks

A major advantage of a circular wave power device in the open sea is the independence of absorption efficiency on the incidence angle. A possible disadvantage is the higher cost of construction, maintenance, energy transmission, storage and the like. We have shown that omnidirectionality can still be achieved by the less expensive installation

at the tip of a very thin breakwater. In practice, this theoretical advantage will of course be reduced,since the thickness of the breakwater is likely comparable to the size of the OWC. As a consequence the opening will be less than 2π, making the averaged response inside the column more sensitive to the incidence angle. A theory accounting for realistic geometry can in principle be carried out by numerical means as in Martins-Rivas & Mei (2007). We have further explored the benefit of air compressibility in broadening the frequency bandwidth of absorption efficiency. Unlike systems in which energy is extracted from the motion of rigid bodies, this benefit is inherent and unique in the pneumatic power takeoff. Finally the exact solution given in Appendix A can be used to study land-based OWC on other types of coasts such as a straight coast and a cape. Further challenges in the design of controllable turbine systems remain.

We acknowledge the financial support by a grant from the Sustainable Energy Program of MIT–Portugal Alliance Project. Partial funding has also been received from US-Israel Bi-National Science Foundation. Discussions with Professors Antonio Falcão and Antonio Sarmento of the Technical University of Lisbon, Portugal, have been especially helpful.

Appendix. Exact theory of diffraction by a solid circular cylinder at the tip of a wedge

Among the analytical techniques for the exact solution of the classical problem of two-dimensional diffraction by a semi-infinite screen (or a wedge), the method by Stoker (1958) can be easily extended to the diffraction by a circular column centred at the tip of a wedge and standing on the seabed. The theory to be derived can be applied to, or modified for, two-dimensional acoustic, elastic or electromagnetic waves.

Let a solid cylinder of radius a be centred at the tip of the wedge defined by $r > a,\ 0 < \theta < \nu\pi$. An incident plane wave approaches from angle α with respect to the x-axis ($\theta = 0$). Since h is constant, the three-dimensional velocity potential can be written as

$$\varphi_1(r, \theta, z) = -\frac{\mathrm{i}gA_0}{\omega}\eta(r, \theta)\frac{Z_0(z)}{Z_0(0)}. \tag{A 1}$$

The normalized free-surface displacement η satisfies the Helmholtz equation in the (x, y) or (r, θ) plane. Following Stoker, we expand η in Fourier series

$$\eta(r, \theta) = \frac{1}{\nu\pi}\bar{\eta}_0(r) + \frac{2}{\nu\pi}\sum_{n=1}^{\infty}\bar{\eta}_n(r)\cos\frac{n\theta}{\nu}, \quad r > a,\ 0 < \theta < \nu\pi, \tag{A 2}$$

where $\bar{\eta}_n$ is the Fourier expansion coefficient of η:

$$\bar{\eta}_n(r, \nu) = \int_0^{\nu\pi}\eta(r, \theta)\cos\frac{n\theta}{\nu}d\theta, \quad n = 0, 1, 2, 3, \ldots . \tag{A 3}$$

On the wedge surfaces $\theta = 0, \nu\pi$ the normal derivative

$$\frac{1}{r}\frac{\partial\eta}{\partial\theta} = -\frac{2}{\nu\pi r}\sum_{n=1}^{\infty}\frac{n}{\nu}\bar{\eta}_n(r)\sin\frac{n\theta}{\nu} \tag{A 4}$$

vanishes for all $r > a$.

From Helmholtz equation governing $\eta(r,\theta)$, the Fourier coefficient $\bar{\eta}_n$ must satisfy Bessel's equation of the order of n/ν, subject to the no-flux boundary condition on the cylinder wall. The solution must be of the form,

$$\bar{\eta}_n = a_n \left(J_{n/\nu}(kr) - \frac{J'_{n/\nu}(ka)}{Y'_{n/\nu}(ka)} Y_{n/\nu}(kr) \right), \tag{A 5}$$

where a_n remains unknown. Since the total potential is the sum of incident η^I and scattered η^S potentials, the finite Fourier transform of the scattered wave is

$$\bar{\eta}_n^S = \bar{\eta}_n - \bar{\eta}_n^I = \bar{\eta}_n - \int_0^{\nu\pi} \eta^I \cos\frac{n\theta}{\nu} \mathrm{d}\theta. \tag{A 6}$$

Since η^S must satisfy the radiation condition, we require

$$\sqrt{r}\left(\frac{\mathrm{d}\bar{\eta}_n^S}{\mathrm{d}r} - \mathrm{i}k\bar{\eta}_n^S \right) \to 0, \quad kr \gg 1. \tag{A 7}$$

It is easily shown from (A 5) that

$$\sqrt{r}\left(\frac{\mathrm{d}\bar{\eta}_n}{\mathrm{d}r} - \mathrm{i}k\bar{\eta}_n \right) \sim a_n \sqrt{\frac{2k}{\pi}} \mathrm{e}^{-\mathrm{i}\left(kr - \frac{n\pi}{2\nu}\right)} \left[\mathrm{e}^{-\mathrm{i}\pi/4} - \mathrm{e}^{\mathrm{i}\pi/4} \frac{J'_{n/\nu}(ka)}{Y'_{n/\nu}(ka)} \right], \quad kr \gg 1. \tag{A 8}$$

For a plane incident wave from angle α with respect to the x-axis, $\eta^I = \mathrm{e}^{\mathrm{i}kr\cos(\theta-\alpha)}$, the method of stationary phase yields

$$\begin{aligned} \sqrt{r}\left(\frac{\mathrm{d}}{\mathrm{d}r} - \mathrm{i}k \right) \bar{\eta}_n^I &= \sqrt{r}\left(\frac{\mathrm{d}}{\mathrm{d}r} - \mathrm{i}k \right) \int_0^{\nu\pi} \mathrm{e}^{\mathrm{i}kr\cos(\theta-\alpha)} \cos\frac{n\theta}{\nu} \mathrm{d}\theta \\ &\sim 2\sqrt{2\pi k} \cos\frac{n\alpha}{\nu} \mathrm{e}^{-\mathrm{i}(kr+\pi/4)} \end{aligned} \tag{A 9}$$

(see Stoker 1958, p. 122). To satisfy (A 7) we equate the two asymptotic approximations above and get

$$a_n \sqrt{\frac{2k}{\pi}} \mathrm{e}^{-\mathrm{i}(kr-(n\pi/2\nu))} \left[\mathrm{e}^{-\mathrm{i}\pi/4} - \mathrm{e}^{\mathrm{i}\pi/4} \frac{J'_{n/\nu}(ka)}{Y'_{n/\nu}(ka)} \right] = 2\sqrt{2\pi k} \cos\frac{n\alpha}{\nu} \mathrm{e}^{-\mathrm{i}(kr+\pi/4)}, \tag{A 10}$$

yielding

$$a_n = \frac{2\pi \cos\frac{n\alpha}{\nu} \mathrm{e}^{-\mathrm{i}n\pi/2\nu} Y'_{n/\nu}(ka)}{Y'_{n/\nu}(ka) - \mathrm{e}^{\mathrm{i}\pi/2} J'_{n/\nu}(ka)} = \frac{2\pi\mathrm{i} \cos\frac{n\alpha}{\nu} \mathrm{e}^{-\mathrm{i}n\pi/2\nu} Y'_{n/\nu}(ka)}{H'_{n/\nu}(ka)}, \tag{A 11}$$

where $H_{n/\nu} \equiv H^{(1)}_{n/\nu}$. In particular if $n = 0$

$$a_0 = \frac{2\pi\mathrm{i} Y'_0(ka)}{H'_0(ka)}. \tag{A 12}$$

In summary the exact solution is

$$\eta = \sum_{n=0}^{\infty} \frac{\epsilon_n}{\nu\pi} \frac{2\pi\mathrm{i} \cos\frac{n\alpha}{\nu} \mathrm{e}^{-\mathrm{i}n\pi/2\nu} Y'_{n/\nu}(ka)}{H'_{n/\nu}(ka)} \left(J_{n/\nu}(kr) - \frac{J'_{n/\nu}(ka)}{Y'_{n/\nu}(ka)} Y_{n/\nu}(kr) \right) \cos\frac{n\theta}{\nu}, \tag{A 13}$$

where $\epsilon_0 = 1$; $\epsilon_n = 2, n = 1, 2, 3, \ldots$, are the Jacobi symbols.

The limiting case $\nu = 2$ gives the diffraction potential for a circular cylinder at the tip of a thin breakwater,

$$\eta = \sum_{n=0}^{\infty} \epsilon_n \frac{\cos\frac{n\alpha}{2} \mathrm{e}^{-\mathrm{i}n\pi/4} \mathrm{i} Y'_{n/2}(ka)}{H'_{n/2}(ka)} \left(J_{n/2}(kr) - \frac{J'_{n/2}(ka)}{Y'_{n/2}(ka)} Y_{n/2}(kr) \right) \cos\frac{n\theta}{2}, \tag{A 14}$$

which can be rewritten as

$$\eta = \sum_{n=0}^{\infty} \epsilon_n \cos\frac{n\alpha}{2} \mathrm{e}^{-\mathrm{i}n\pi/4} J_{n/2}(kr) \cos\frac{n\theta}{2} + \sum_{n=0}^{\infty} \epsilon_n \cos\frac{n\alpha}{2} \mathrm{e}^{-\mathrm{i}n\pi/4} \left[\left(\frac{\mathrm{i} Y'_{n/2}(ka)}{H'_{n/2}(ka)} - 1 \right) J_{n/2}(kr) - \mathrm{i} \frac{J'_{n/2}(ka)}{H'_{n/2}(ka)} Y_{n/2}(kr) \right] \cos\frac{n\theta}{2}. \tag{A 15}$$

The first series is the effect of the semi-infinite breakwater; the second is the additional effect of the cylinder. In the limit of $ka \to 0$, the second series disappears. The special case of $\nu = 1$ corresponds to a half-cylinder on a straight coast. This result can be reduced to one found more easily by the method of images. The solution for a cylinder connected to a wedge of any other angle can also be found from the general result here.

REFERENCES

Budal, K. & Falnes, J. 1977 Optimum operation of improved wave-power converter. *Marine Sci. Comm.* **3**, 133–150.

Erdélyi, A., Magnus, W. Oberhettinger, F. & Tricomi, F. G. 1954 *Tables of Integral Transforms 1.10*. McGraw-Hill.

Evans, D. V. 1976 A theory for wave power absorption by oscillating bodies. *J. Fluid Mech.* **77**, 1–25.

Evans, D. V. 1978 The oscillating water column wave energy device. *J. Inst. Math. Appl.* **22**, 423–433.

Evans, D. V. 1981 Power from water waves. *Annu. Rev. Fluid Mech.* **13**, 157–187.

Evans, D. V. 1982 Wave-power absorption by systems of oscillating surface pressure distributions. *J. Fluid Mech.* **114**, 481–99.

Evans, D. V. 1988 The maximum efficiency of wave-energy devices near coast lines. *Appl. Ocean Res.* **10**, 162–164.

Evans, D. V. & Porter, R. 1995 Hydrodynamics characteristics of an oscillating water column device. *Appl. Ocean Res.* **17**, 155–164.

Evans, D. V. & Porter, R. 1997 Efficient calculation of hydrodynamic properties of OWC-type devices. *J. Offshore Mech. Arctic Engng* **119**, 210–218.

Falcão, A. F. de O. 2000 The shoreline OWC power plant at the azores. In *Fourth European Wave Energy Conf*., Aalborg, Denmark.

Falcão, A. F. de O. 2002 Control of an oscillating-water-column wave power plant for maximum energy production. *Appl. Ocean Res.* **24**, 59–71.

Falcão, A. F. de O. & Sarmento, A. J. N. A. 1982 Wave generation by a periodic surface pressure and its application in wave-energy extraction. In *Fifteenth Intl Cong. on Theor. Appl. Mech.*, Toronto, Canada.

Falnes, J. 2002 *Ocean Waves and Oscillating Systems*. Cambridge University Press.

Garrett, C. J. R. 1970 Bottomless harbours. *J. Fluid Mech.* **43**, 433–449.

Heath, T. V. 2007 The development of a turbo-generation system for application in an OWC breakwater. In *Seventh European Wave and Tidal Energy Conf*., Porto, Portugal.

Martins, E., Siveira Ramos, F., Carrilho, L., Justino, P., Gato, L., Trigo, L. & Neumann, F. 2005 Ceodouro project: overall design of an OWC in the new Oporto breakwater. In *Sixth European Wave and Tidal Energy Conf*., Glasgow, UK.

Martins-Rivas, H. & Mei, C. C. 2007 Diffraction effects near Foz do Douro breakwater. In *Proc. oF the Seventh European Wave and Tidal Energy Conf*., Porto, Portugal.

McCormick, M. E. 1981 *Ocean Wave Energy Conversion*. Wiley Interscience.

McIver, P. & Evans, D. V. 1988 An approximate theory for the performance of a number of wave-energy devices set into a reflecting wall. *Appl. Ocean Res.* **10**, 58–65.

Mei, C. C. 1976 Power extraction from water waves. *J. Ship Res.* **20**, 63–66.

Mei, C. C. 1983 *The Applied Dynamics of Ocean Surface Waves*. Wiley.

Newman, J. N. 1979 Absorption of wave energy by elongated bodies. *Appl. Ocean Res.* **1**, 189–196.

Salter, S. H. 1974 Wave power. *Nature* **249**, 720–724.

Sarmento, A. J. N. A. & Falcão, A. F. de O. 1985 Wave generation by an oscillating surface-pressure and its application in wave-energy extraction. *J. Fluid Mech.* **150**, 467–485.

Smith, C. M. 1983 Some problems in linear water waves. PhD thesis, University of Bristol.

Stoker, J. J. 1958 *Water Waves*. Wiley Interscience.